Fluid model for a partially packed dielectric barrier discharge plasma reactor

Siddharth Gadkari,[1] Xin Tu,[2] and Sai Gu[1, a)]

[1)] *Department of Chemical and Process Engineering, University of Surrey, Guildford GU2 7XH, UK*

[2)] *Department of Electrical Engineering and Electronics, University of Liverpool, Brownlow Hill, Liverpool L69 3GJ, UK*

In this work, a two-dimensional numerical fluid model is developed for a partially packed dielectric barrier discharge (DBD) in pure helium. Influence of packing on the discharge characteristics is studied by comparing the results of DBD with partial packing with those obtained for DBD with no packing. In the axial partial packing configuration studied in this work, the electric field strength was shown to be enhanced at the top surface of the spherical packing material and at the contact points between the packing and the dielectric layer. For each value of applied potential, DBD with partial packing showed an increase in the number of pulses in the current profile in the positive half cycle of the applied voltage, as compared to DBD with no packing. Addition of partial packing to the plasma-alone DBD also led to an increase in the electron and ion number densities at the moment of breakdown. The time averaged electron energy profiles showed that a much higher range of electron energy can be achieved with the use of partial packing as compared to no packing in a DBD, at the same applied power. The spatially and time averaged values over one voltage cycle also showed an increase in power density and electron energy on inclusion of partial packing in the DBD. For the applied voltage parameters studied in this work, the discharge was found to be consistently homogeneous and showed the characteristics of atmospheric pressure glow discharge.

[a)] Electronic mail: sai.gu@surrey.ac.uk

I. INTRODUCTION

Packed bed dielectric barrier discharge (DBD) is being increasingly used as a chemical reactor for remediation of environmental pollutants (e.g. NOx, SOx, VOCs.), and conversion of greenhouse gases to useful chemicals[1,2,3]. The non-equilibrium nature of DBD provides major advantage, by allowing operation at atmospheric pressure and ambient conditions. This helps to overcome the thermodynamic barriers in chemical reactions and provides high reactivity at room temperatures[4,5]. In cases, when the packing material is a catalyst, the so called 'plasma-catalysis' provides a synergistic effect and also helps to improve the selectivity towards desirable products[2,6]. Additional features such as easy operation, moderate capital cost and simple scalability have led to extensive research on packed bed DBDs[7].

Several studies which have used packing material in conjunction with plasma in a DBD have found enhanced performance in comparison to a plasma alone system[2,3,6,8,9,10,11,12], however many studies have also reported a negative impact on the performance[9,13,14,15]. This unfavorable response has been shown to be related to packing configuration and the void fraction of the discharge in the packed bed DBD[16]. It has been observed that in a fully packed DBD, which provides a very low void fraction, the packing leads to a significant change in discharge behaviour. It reduces the amplitude of the current pulses and changes the typical filamentary mode of discharge observed in a plasma-alone DBD to a prevalent surface discharge on the packing surface and spatially limited microdischarges[16,17,18]. Suppression of the filamentary discharges in a fully packed DBD was suggested to be responsible for the negative performance[16]. An alternative packing configuration, in which the packing material (catalyst particles or dielectric pellets) are placed along the bottom of the dielectric barrier layer over the entire length of the discharge (partial packing), was evaluated[16,19,20]. It was found that such a packing configuration provided a large void fraction and exhibited strong filamentary microdischarges in the discharge gap without causing any significant change to the discharge mode. Partially packed DBD thus induces effective plasma-catalyst interactions, which may generate a synergistic effect and hence promote plasma-catalytic chemical reactions[16,19,20].

Improvement of performance in either partial or fully packed bed DBD is typically attributed to the effective polarization and enhanced electric field strength at the contact points and in some cases to the synergistic effect of plasma-catalysis, however the exact

fundamental mechanisms are still not fully understood[16,21,22]. Several experimental studies have been attempted to investigate the nature of physical and chemical interactions between packing materials and plasma in packed DBDs[22,23,24]. However experimental studies have their limitations in terms of parameters that can be accurately measured during plasma operation, and the packing itself adds an extra impediment in visibility for optical/laser analysis. And while such experimental diagnostic studies are indispensable, we believe computational modeling can be used as a complimentary tool to optimize the system in a directed way, providing more quantitative process-parameter relationships[25].

In the last two decades, some computational studies have been performed for packed bed DBD reactors[21,26,27,28,30,31,32,33]. Takaki et al.[31] developed a one-dimensional physical model for ferroelectric packed bed barrier discharge reactor in a pure nitrogen environment and found that all the plasma parameters increase linearly with applied ac voltage and pellet dielectric constant. Kang et al.[26] carried out a numerical study of ferroelectric packed discharge (FPD) using a 2 D finite-element method (FEM) model considering single and double pellet cases. Their model however did not include any plasma chemistry and was limited to nano-second time-scale. Russ et al.[30] developed a 2D fluid model for a packed bed DBD filled with synthetic, dry exhaust gas (80% N, 20% O, and 500 ppm NO) at atmospheric pressure for simulation of transient microdischarges based on the so-called 'donor cell' method. While this study included comprehensive plasma chemistry, it presented very short one-directional discharge (of a few 10s of nanoseconds) with limited results of spatial electric field and electron density distributions[30]. Van Laer and Bogaerts[21] developed a fluid model for a packed bed dielectric barrier discharge plasma reactor using two complementary axisymmetric 2D geometries and pure helium gas plasma chemistry. Their results showed enhancement in electric field and electron energy due to effective polarization of the beads in the packed bed. They also observed a change in discharge mode (from Townsend to glow mode) on increasing the applied potential. In a later study, Van Laer and Bogaerts[32] studied the influence of the dielectric constant of the packing on the plasma characteristics, for two different gap sizes using a 2D axisymmetric fluid model. They observed that a stronger discharge is obtained in a microgap reactor and that increasing dielectric constant of the beads enhances the electric field strength but only up to a certain extent. In addition to fluid models, some other modelling strategies have also been used to study the propagation of microdischarges in packed bed DBD, such as 2D particle-in-cell/Monte Carlo technique,

multi-fluid simulator nonPDPSIM code, etc.[27,33].

Although fully packed DBD systems have been well investigated both experimentally and numerically, the same cannot be said about partially packed DBDs. Therefore in this work, for the first time, we have developed a 2D fluid model to understand the discharge characteristics in a partially packed DBD and compared the discharge parameters with that of a plasma-alone DBD reactor with no packing.

The paper is structured as follows: geometry and mathematical model used in the analysis including the respective governing equations and boundary conditions, are described in section 2. Results obtained from the analysis, including the discharge current profiles, spatial distribution profiles of electric field strength, electron and ion density and time averaged electron energy plots are presented and discussed in section 3. Section 4 summarizes the final conclusion of this study.

II. MODEL DESCRIPTION

A. Geometry

In this work, the co-axial DBD plasma reactor is modeled using a 2-D fluid model in COMSOL Multiphysics[29]. The model is applied to a cylindrical DBD reactor with two co-axial metal cylinders as electrodes. The inner electrode is connected to a high voltage AC power supply and the outer electrode is grounded. The diameters of the internal and external cylinders of the DBD reactor are 16 mm and 23 mm respectively. The outer electrode is covered (on the inside) with a 1.5 mm dielectric barrier layer of alumina (relative permittivity, $\epsilon_r = 9$). The discharge is sustained in the 2 mm co-axial gap between the inner electrode and the alumina layer. The length of the electrodes is 100 mm. These dimensions represent a generic geometry, based on the wide range of DBD reactors with different discharge gaps, dielectric layer thickness and electrode lengths that have been used as chemical reactors in several experimental studies[20,34,35].

The partial packing approach[16,19,20] has been adopted in the work and a layer of catalyst particles is packed along the bottom of the discharge tube (on top of the dielectric layer). Ni-Al_2O_3 ($\epsilon_r = 50$) is used as a representative packing particle in the model[14,16,36]. Particles are assumed to be perfectly spherical for simplicity and unless mentioned otherwise, the

particle diameter is 1 mm. Also as the particles are fixed on the top of the dielectric layer using quartz wool, it is assumed that the particles are not touching the surface with a point edge. While the fixing material (such as quartz wool) may have an effect on the plasma discharge, such an effect is neglected in this analysis. A 3D representation of a section of the partially packed co-axial DBD reactor, is shown in figure 1.

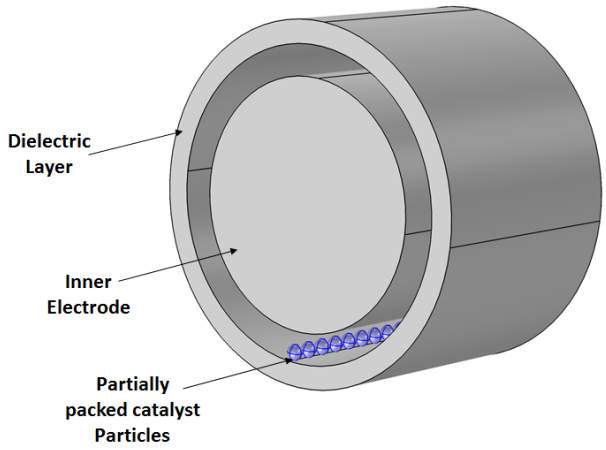

FIG. 1. 3D representation of the partially packed co-axial DBD.

A full 3D simulation of the DBD will be able to replicate the real system and provide a thorough understanding of the effect of packing on the discharge behaviour. However due to complexity of the equations involved and considering the current computational constraints, it will be impractical to run a 3D simulation[21]. Thus in this study we have used a representative 2D model by considering a small section of the DBD reactor, which includes the inner and outer electrode boundaries, the discharge gap, dielectric barrier and two packing particles. The final 2D geometries of the DBD (both with and without catalyst packing) used in the model are shown in figure 2. Symmetry of catalyst particles aligned axially is used and only half section of the each catalyst is represented (figure 2a). The selected geometry helps in reducing the computational size of the model while also allowing to analyze the discharge in the region between two particles.

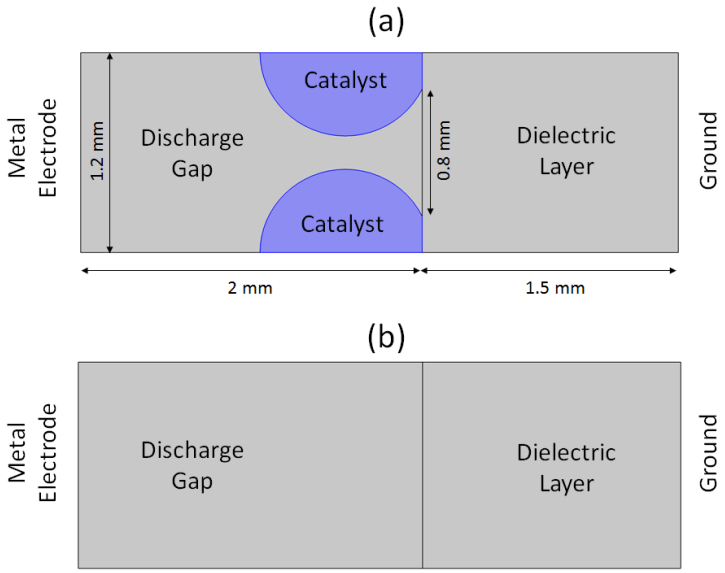

FIG. 2. 2D geometries of the DBD used in the model, (a) with partial packing, (b) without packing.

The typical target molecules in gas cleaning applications in co-axial DBD reactors are NOx, SOx, CH_4, CO_2, Toluene, Naphthalene, etc. However the plasma chemistries of these molecular gases frequently involves tens of species and hundreds or even thousands of reactions including the electron impact, electron-ion recombination, neutral-neutral, ion-neutral and ion-ion reactions, etc.[24,37]. Solving fluid models with such complex chemistries is computationally very expensive, particularly on a 2D geometry. Thus in this study we have decided to use pure helium as the discharge gas. Helium, has a relatively simpler plasma chemistry, low breakdown voltage and ionizes easily to form a stable homogeneous glow discharge, which is easier to simulate using a fluid model, as opposed to the filamentary discharge typically observed with molecular gases[4,38,39]. These factors further help in reducing the model size and the computational cost, thereby providing more leverage in performing a longer study over more periods of applied potential such that stable behaviour can be studied. It should be noted, that the difference in discharge performance between helium and molecular gases also limits the applicability of the current model. However using helium is a good starting point and helps in expanding our understanding of the partially packed DBDs, which will be useful in future investigations of the same.

B. Governing Equations and Boundary Conditions

Governing equations describing the fluid theory originate by solving a set of moments of the Boltzmann equation[4]. Typically for most applications, the first three moments are considered, that describe the particle, momentum and energy conservation. By taking these moments, the Boltzmann equation is reduced to a 3-dimensional, time dependent problem and describes the plasma in terms of averaged quantities such as density, momentum and mean energy[4,40].

The zeroth moment of the Boltzmann equation gives the the continuity equation describing the rate of change of particles (electrons, ions or neutral species) :

$$\frac{\partial}{\partial t}\left(n_p\right) + \vec{\nabla} \cdot \vec{\Gamma}_p = R_p \tag{1}$$

The subscript p refers to different species such as electrons, ions or neutral species. n represents the density of species, $\vec{\Gamma}$ represents the flux vector and R_p represents either the source/sink term and accounts for the production or loss of a particular species p in chemical reactions, ionization events, etc. Losses at the walls are accounted in the boundary conditions and are not explicitly considered in the particle continuity equation.

In the fluid model, the first moment of the Boltzmann equation is not solved explicitly but is replaced by another simplification known as the drift diffusion approximation[4,40], which is used to derive the flux term in equation 1.

Flux term for the particles (based on drift-diffusion approximation) consists of a diffusion term and a drift term, given as,

$$\vec{\Gamma}_p = \pm n_p \mu_p \vec{E} - D_p \cdot \vec{\nabla} n_p \tag{2}$$

where, E refers to the electric field, μ and D refer to the mobility and diffusion coefficient of the species respectively, and their values have been taken from Ref[21]. The first term of equation 2 is zero for the neutral species.

Source/sink term, R_p is calculated as,

$$R_p = \sum \left(c_{pj} r_{pj}\right) \tag{3}$$

where c_p represents the stoichiometric coefficient and r_p represents the reaction rate of the target species for reaction j.

The second moment of the Boltzmann equation is used to derive the energy conservation equation. The final expression for rate of change of electron energy density including the drift diffusion approximation is described as,

$$\frac{\partial}{\partial t}\left(n_\epsilon\right) + \vec{\nabla}\cdot\vec{\Gamma_\epsilon} + \vec{E}\cdot\vec{\Gamma_e} = R_\epsilon \tag{4}$$

where, n_ϵ is the electron energy density, R_ϵ is the energy loss/gain due to inelastic collisions. The flux vector for electron energy $\vec{\Gamma_\epsilon}$ is given as,

$$\vec{\Gamma_\epsilon} = -\frac{5}{3}\left(\mu_e\cdot\vec{E}\right)n_\epsilon - \frac{5}{3}\vec{\nabla}D_e n_\epsilon \tag{5}$$

A self-consistent electric field distribution is calculated by solving the Poisson's Equation (equation 6) in the plasma region and the Laplace's Equation (equation 7) in the dielectric material.

$$-\vec{\nabla}\cdot\epsilon_0\epsilon_r\vec{\nabla}V = \rho \tag{6}$$

$$-\vec{\nabla}^2 V = 0 \tag{7}$$

$$E = -\vec{\nabla}V \tag{8}$$

where ϵ_0 is the permittivity of free space, ϵ_r the relative permittivity, ρ the space charge density ($\mathrm{C/m^3}$) and V the applied potential.

Surface charge accumulation on the dielectric layer due to difference in fluxes between the electrons and ions is taken into account using the following boundary conditions,

$$-n\cdot\left(\vec{D_1}-\vec{D_2}\right) = \rho_s \tag{9}$$

$$\frac{d\rho_s}{dt} = n\cdot\vec{J_i} + n\cdot\vec{J_e} \tag{10}$$

where n is the unit normal, ρ_s is the surface charge density, $\vec{D_1}$ and $\vec{D_2}$ are the electric displacement fields on both sides of the boundary, $\vec{J_i}$ and $\vec{J_e}$ are the total ion and electron current densities at the wall.

A set of 23 reactions involving helium atoms (He), ions (He^+ and He_2^+), metastables (He^* and He_2^*) and electrons is used the model[21]. At the walls helium metastables quench and change back to neutral helium atoms. Helium ions too change back to neutral helium atoms while emitting secondary electrons with emission coefficient of 0.05 and mean energy 5 eV[21]. Gas temperature is assumed to be constant at 300 K. Discharge is driven by applying a sinusoidal electric potential to the inner cylinder with different values of applied voltage

amplitude at a fixed frequency of 20 kHz. Initial densities of electrons and ions are assumed as spatially uniform and set as 10^{14} m^{-3}.

A sinusoidal electric potential (V) is applied to the top boundary (inner electrode),

$$V = V_0 \sin(\omega t) \tag{11}$$

where V_0 is the applied peak voltage and ω is the angular frequency. The RF frequency value is kept constant at 20 kHz. The electric potential at the exterior boundary of the dielectric barrier (bottom boundary) is 0 V.

III. RESULTS & DISCUSSION

The model developed in this study is first validated with an experimental result published in a previous study by Tu et al.[41] for a helium DBD. Figure 3 shows the comparison of discharge current profiles obtained from an experimental study[41] with that predicted by the model developed in this study for a helium DBD with no packing with the same set of operating parameters and reactor geometry. Since the 2D simulation is being performed on a small section of the co-axial DBD reactor, it should be noted that the predicted value of current obtained from the simulation needs to be multiplied by a factor to account for the total height and circumference of the reactor. Also, the model was run until stable predictions could be obtained and in this particular case the simulation predictions had stabilized by the 3rd period of applied voltage. The predicted discharge current profile shown in figure 3B is that obtained for the 4th period of applied voltage. As can be seen from figure 3, the predicted discharge current profile may not exactly overlap the one observed in the experimental study, still reasonable agreement is obtained between the two. Also, the magnitude of current and the position of the major current peaks in the positive and negative half cycles of applied potential predicted by the numerical analysis are in fairly good agreement with that obtained from the experimental study. This is particularly encouraging, as real systems typically have at least some fraction of impurities in the helium gas, whereas in the model we have assumed a pure helium discharge gas. For DBD with partial packing, the numerical results cannot be directly compared with experimental studies at this point, as all the reported studies on partially (axial) packed DBDs have used molecular gases[16,19,20] and not helium. However we have attempted to draw qualitative comparisons of discharge characteristics with relevant experimental studies, as the results are discussed ahead.

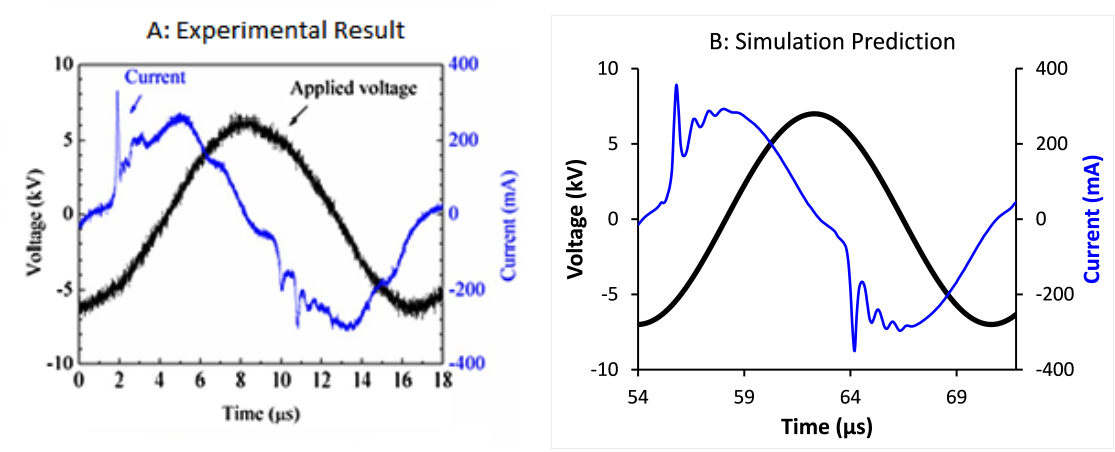

FIG. 3. Comparison of discharge current profile (blue lines) obtained from (A) experimental study by Tu et. al.[41] with (B) simulation predictions from the model developed in this study, for one voltage cycle (black lines) at a frequency of 60 kHz in a helium DBD without any packing. (Experimental result (A) has been reprinted with the permission from Phys. Plasmas, 18(8):080702, (2011)[41]. Copyright 2011 AIP Publishing.)

Results obtained from the numerical analysis, comparing the plasma-alone DBD with a DBD with partial packing are presented next. Figure 4 shows the discharge current profiles in helium DBD without any packing and with partial packing during one cycle of the applied potential of 3 kV peak-to-peak at a frequency of 20 kHz. As can be seen from figure 4A, for helium DBD with no packing, the current profile exhibits a single distinct pulse in both the positive and negative half cycle of the applied voltage. Such a current profile is characteristic of helium DBD operating under homogeneous mode and is referred to as the atmospheric pressure glow discharge (APGD)[42]. This will be be further confirmed ahead, as we discuss the typical electron and ion densities observed in APGD. It should also be noted that the current profiles for DBD with no packing, for frequencies, 20 kHz (figure 4a) and 60 kHz (figure 3b) are quite different. At the higher frequency, 60 KHz, the current profile exhibits a sinusoidal shape, much different from the standard pulse-like waveform observed for atmospheric DBDs[38]. Such a distinct difference in current profiles at higher frequencies has been observed before[43,44] and has been attributed to the constant production of charged particles due to continuous existence of excited species at higher frequencies[44].

On inclusion of partial packing, discharge current profile (figure 4B) changes in the pos-

itive half cycle, showing two current peaks (of successively decreasing amplitude). These current peaks are marked 1 and 2 in the figure 4B. Helium DBD exhibiting multiple pulses in the discharge current profiles is said to be operating as pseudo-glow discharge[45]. Such an increase in current peaks on inclusion of catalyst packing in helium DBD has been previously observed by Tu et.a al.[41] for a DBD with radial partial packing of Al_2O_3 compared to DBD with no packing. Tu and Whitehead[16] also observed an increase in current pulses with radial and axial partial packing of Ni/γ-Al_2O_3 in co-axial DBD reactor during dry reforming of CH_4. The increase in current pulses is typically attributed to the increase in charge density due to additional charge deposition on the surface of the catalyst packing material[16,41]. The discharge ignites once the gap voltage reaches the breakdown voltage and extinguishes once the gap voltage falls below the breakdown voltage. This is expressed in the current signal in the form of a peak. Multiple peaks occur due to multiple breakdown in a single voltage cycle[38,45], which can happen if the gap voltage crosses the breakdown voltage more than once in one cycle. Large accumulation of charges increases the external voltage significantly, making multiple breakdowns feasible[46].

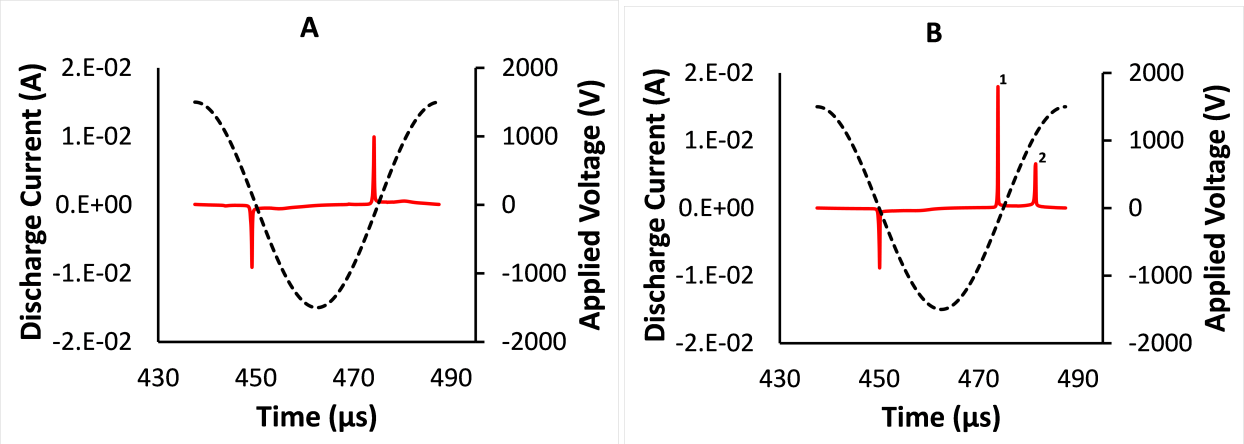

FIG. 4. Discharge current profiles (red solid lines) in an atmospheric DBD in helium (A) without packing and (B) with partial packing, during once cycle of the applied potential of 3 kV peak-to-peak (black dashed lines) at a frequency of 20 kHz.

In addition to undergoing this transition from single peak to multi-peak behaviour in the positive half cycle of applied voltage, the amplitude of the current pulses for DBD with partial packing also increases in comparison to DBD without any packing. This signifies a

stronger discharge and is in accordance with previously reported studies[16,41], where a slight increase in current amplitude is observed on use of catalyst packing.

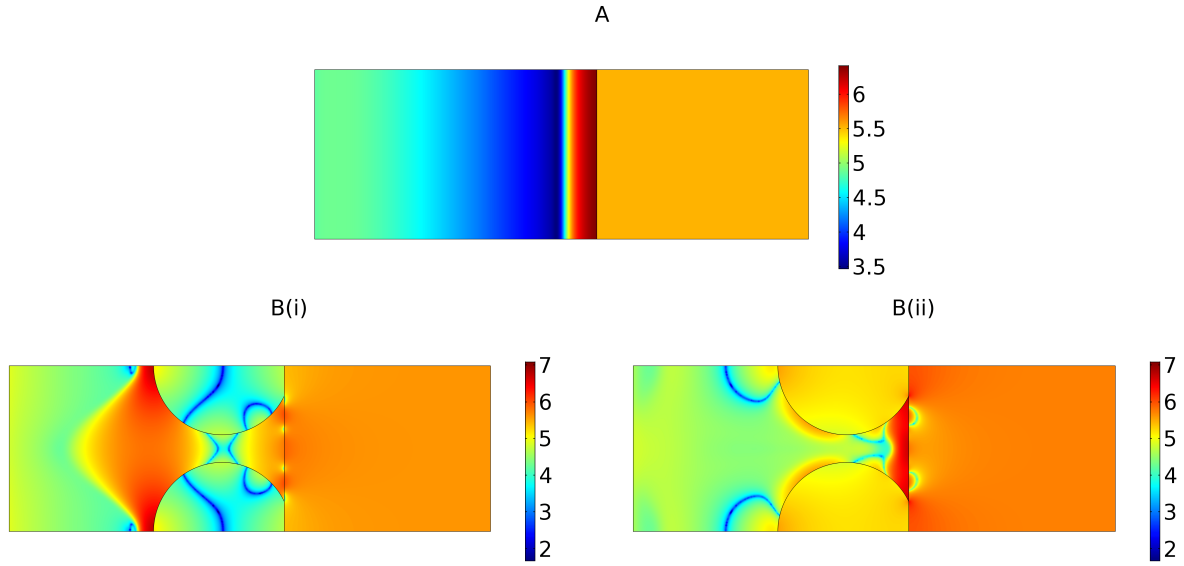

FIG. 5. Logarithm to the base 10 of electric field strength (V/m) at the moment of gas breakdown in (A) DBD with no packing, corresponding to time at current peak (474.2 μs) of figure 4A above and (B) DBD with partial packing corresponding to time at Peak 1 and Peak 2 as seen in figure 4B above.

Figures 5, 6, 7 and 8 show the electric field strength, space charge density, electron number density, and ion number density distributions at the moment of breakdown during the positive half cycle of the voltage period, corresponding to times shown in figure 4. Accordingly in these three figures, we obtain one distribution profile (A) for the DBD with no packing and two distribution profiles (B (i & ii)) for DBD with partial packing. As can be seen in figures 5A, 7A and 8A; electric field, electron density and ion density spatial distributions in the helium DBD with no packing exhibit characteristics similar to that of low pressure glow discharge[47,48,49]. As expected three distinct regions are observed between cathode to anode, namely cathode fall, negative glow space, and positive column region. In figure 5A, at the point of breakdown, the electric field is maximum at the instantaneous cathode, and linearly decreases in the cathode fall region. Following this, it decreases to its lowest point in the negative glow region, then rises subsequently to an intermediate value and remains uniform in the positive column region. Electron density profile, as seen in figure

7A, shows a distinct cathode fall region near cathode at the moment of breakdown, where a low intensity electron density region is observed. Accordingly ion density is maximum near the cathode and is higher than the maximum electron density at the moment of breakdown, as can be seen in figure 8A.

Figures 5B(i) and 5B(ii) show the electric field distributions corresponding to the two breakdown moments during the positive half cycle of the applied voltage as shown in figure 4B. Comparing with electric field distribution for DBD with no packing (figure 5A), it can be seen that the electric field is deformed due to presence of the packing and the field strength is slightly higher for DBD with partial packing. At the first breakdown point, the electric field strength is maximum at the top surface of the packing particles (figure 5B(i)). Spherical dielectric objects in an electric field produce an intensification of the electric field in the gas at the poles of the solid object and a local minima at the equatorial plane. The intensification is maximum when the electric field is perpendicular to the surface of the solid object[50,51]. In the given configuration of the DBD and spherical packing particles, this enhancement in electric field occurs at the vertical poles, which is the top surface of the particles and a region of low electric field strength can be observed in the area between the two particles where the distance between them is minimum (this is the equatorial plane in the given configuration).

On the other hand, at the moment of second breakdown, the electric field strength is maximum at the contact points between the packing particles and dielectric barrier, as can be seen from figure 5B(ii). This enhancement is typically attributed to increased charge deposition due to more effective polarization at the packing and dielectric barrier surfaces. Similar enhancement in electric field strength at the poles of packing material and at the contact points between packing and dielectric layer has been reported in previous studies on packed bed DBDs[21,26,27,32,50,52].

Figure 6 shows the spatial distribution of space charge density (C m^{-3}) at the moment of breakdown during the positive half cycle of the voltage period, for DBD with no packing and with partial packing, corresponding to the breakdown moments during the positive half cycle of the applied voltage as shown in figure 4. As can be seen from figure 6, the space charge density corresponding to the two current peaks for DBD with partial packing is consistently higher than that obtained for DBD with no packing, which also suggests an improvement in ionization by addition of partial packing at the same applied potential.

The main contribution to the space charge comes from positive ions, and at the moment of breakdown for DBD with no packing, high density of space charge is located near the dielectric layer. For DBD with partial packing however, at the moment of first peak the maximum space charge is located at the top surface of the packing beads (figure 6 B (i)), corresponding to the high electric field strength at this point. The accumulated charge then moves away from the top surface towards the space between the beads near the dielectric layer and a second maxima of charge density is obtained at moment of second breakdown (figure 6 B (ii)). Here the space charge density decreases slightly but manages to induce an electric field such that the gap voltage reaches the breakdown voltage again, within the same voltage period causing a second breakdown.

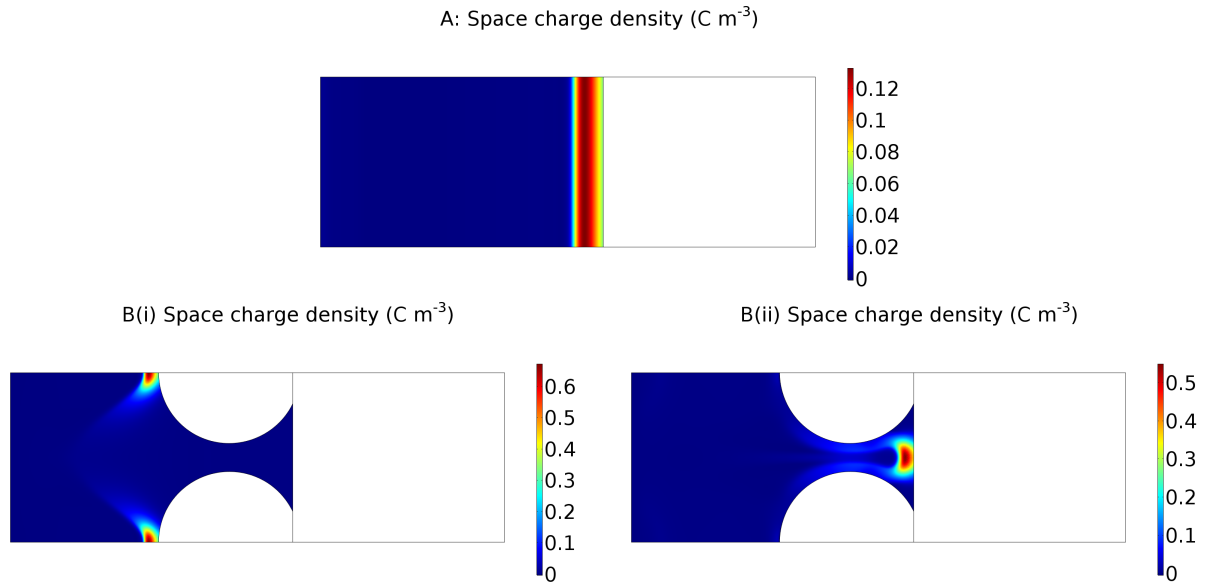

FIG. 6. Space charge density (C m^{-3}) at the moment of gas breakdown in (A) DBD with no packing, corresponding to time at current peak (474.2 μs) of figure 4A above and (B) DBD with partial packing corresponding to time at Peak 1 and Peak 2 as seen in figure 4B above.

Figures 7B(i) and 7B(ii) correspond to the electron density distributions at the two breakdown moments during the positive half cycle of the applied voltage as seen in figure 4B. At the moment of first breakdown for DBD with partial packing, a distinct low electron density region extends from the dielectric barrier surface up to the top surfaces of the packing particles, in a shape reminiscent of the electric field distribution as seen in figure 5B(i). This area exhibits characteristics of the cathode fall region and the distinct pointy

knob shape of this region is probably obtained due to electric field distortion caused by the curvatures of the adjacent spherical packing particles. After this cathode fall region, the maximum electron density is obtained at the top surface of the two particles (figure 7B(i)). At the moment of second breakdown (figure 7B(ii)), a long cylindrical region of high electron density is observed in the region in between the two packing particles, starting slightly above the dielectric barrier layer and extending up to the height of the packing. The cathode fall region, at the moment of second breakdown is only limited to the immediate region close to the barrier layer and packing particles.

By comparing the electron density distributions, it can be seen that the maximum electron density at both the breakdown moments for DBD with partial packing (figure 7B) is roughly about one order of magnitude higher than that observed at the breakdown for DBD with no packing (figure 7A). It should also be noted that the maximum electron density at the moment of first breakdown ($\sim$ 3x10^{12} cm^{-3}) is slightly higher compared to that at the second breakdown ($\sim$ 2.5x10^{12} cm^{-3}) for DBD with partial packing. Comparatively, the maximum electron density for DBD with no packing ($\sim$ 5x10^{11} cm^{-3}) is lower than the maximum electron density at both the breakdown moments for DBD with partial packing.

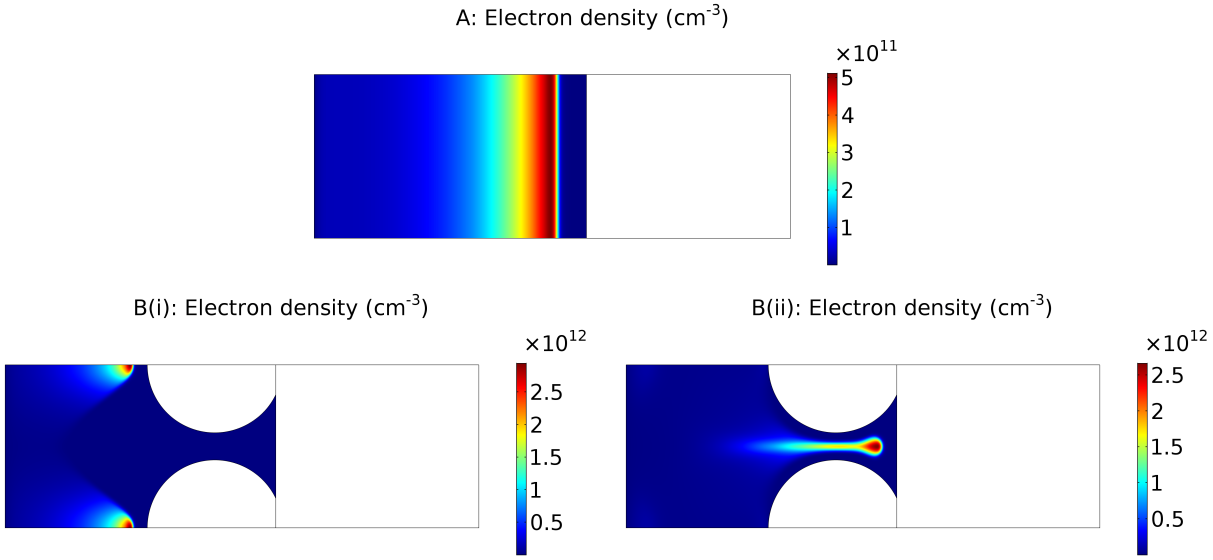

FIG. 7. Electron Density (cm^{-3}) at the moment of gas breakdown in (A) DBD with no packing, corresponding to time at current peak (474.2 μs) of figure 4A above and (B) DBD with partial packing corresponding to time at Peak 1 and Peak 2 as seen in figure 4B above.

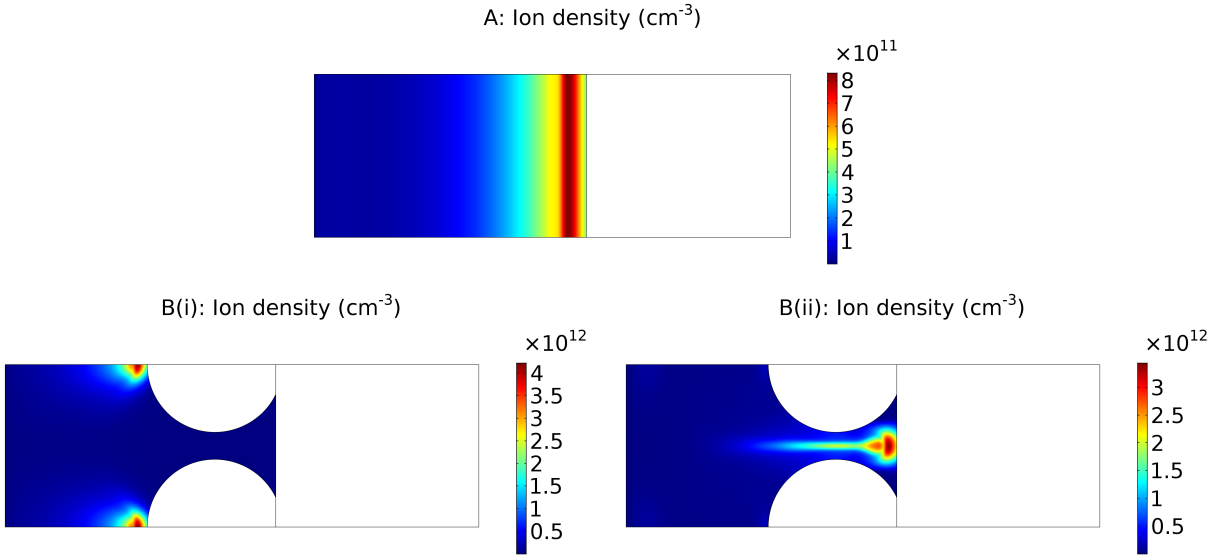

FIG. 8. Ion Density (cm^{-3}) at the moment of gas breakdown in (A) DBD with no packing, corresponding to time at current peak (474.2 μs) of figure 4A above and (B) DBD with partial packing corresponding to time at Peak 1 and Peak 2 as seen in figure 4B above.

Figures 8B(i) and 8B(ii) show the ion density distributions at the two breakdown moments during the positive half cycle of the applied voltage as seen in figure 4B for DBD with partial packing. By comparing the plots, it can be seen that the maximum ion density at both the breakdown moments for DBD with partial packing is higher in magnitude than that observed at the breakdown for DBD with no packing (figure 8A). Similar to the electron density distribution profiles for DBD with partial packing, ion density distribution at the moment of first breakdown shows maximum ion density at the top surface of the packing particles (figure 8B(i)) and at the second breakdown the maximum is observed in the region between the two particles (figure 8B(ii)).

Comparing figures 7 and 8, it can be seen that the ion density is always higher compared to the corresponding electron density for both DBD with packing and with no packing. This is another characteristic feature of the APGD, which is found valid for both the configurations. Typical electron and ion densities for APGD are in the range of 10^{10}-10^{11} cm^{-3} and 10^{11}-10^{12} cm^{-3} respectively[53,54].The electron and ion densities for both the DBD configurations studied in this work, fall within the typical range observed for APGD, further confirming the occurrence of homogeneous discharge.

As the major difference in discharge current profiles for the DBDs with and without packing is seen in the positive half cycle of the applied voltage (3kV peak-to-peak), we wanted to see how this difference is reflected in terms of average electron energy, which is an important factor in determining the decomposition efficiency of the DBD reactor. Figure 9 shows the time averaged electron energy distribution during the positive half cycle of applied potential of 3.0 kV peak-to-peak for both DBD without any packing and DBD with partial packing.

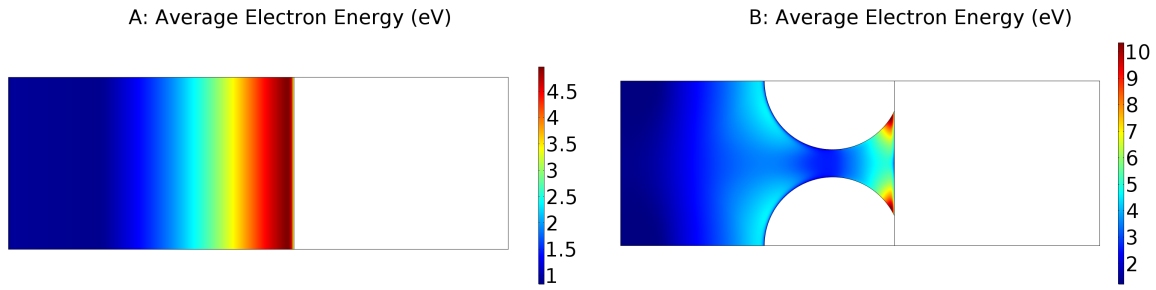

FIG. 9. Time averaged electron energy (eV) distribution during the positive half cycle for applied potential of 3.0 kV peak-to-peak as shown in figure 4 for (A) DBD with no packing and (B) DBD with partial packing.

As can be seen from the figure 9A, for DBD with no packing the maximum electron energy during the half voltage cycle is just below 5 eV and is observed near the instantaneous cathode close to the dielectric surface. On the other hand, for DBD with partial packing (figure 9B) the maximum electron energy during the half voltage cycle is close to 10eV, which is twice of that obtained for DBD when no packing is used. The maximum electron energy ($\sim$ 10eV) is observed at the contact points between the packing material and the dielectric barrier. The electron energy is also significantly higher ($\sim$ 5eV) on the surface of the packing material except in the small region where the distance between the packing beads is minimum. The enhancement in electric field strength at the top surface of the packing particle and at the contact points between the barrier layer and the packing, induces a higher electron energy in these regions and thus the half-period time averaged electron energy distribution in figure 9 shows enhanced electron energy in these areas.

On application of a higher applied potential, 6 kV peak-to-peak, the discharge behaviour changes to a certain extent, more in the case of partially packed DBD. Figure 10 shows the

discharge current profiles in helium DBD without any packing and with partial packing, during one cycle of the applied potential of 6 kV peak-to-peak at a frequency of 20 kHz.

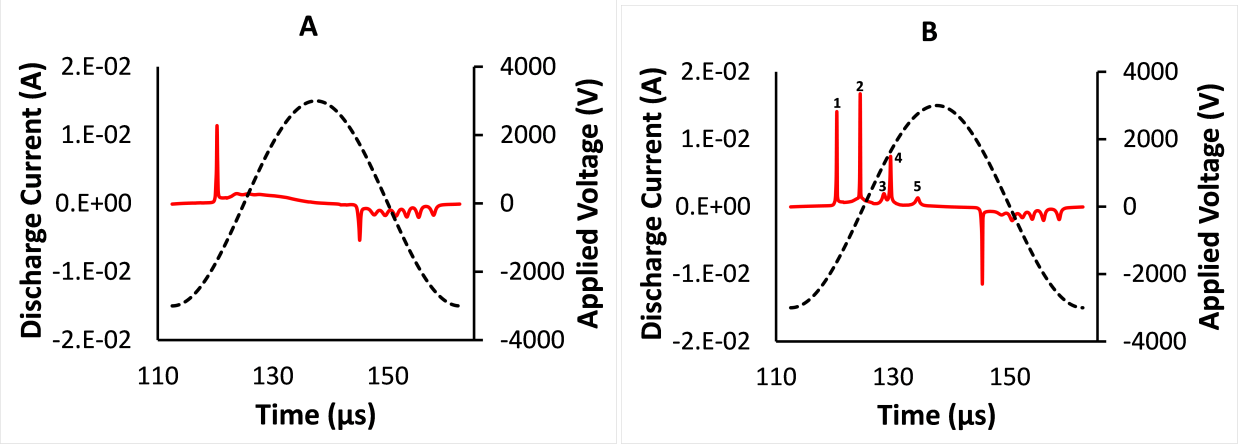

FIG. 10. Discharge current profiles (red solid lines) in an atmospheric DBD in helium (A) without packing and (B) with partial packing, during once cycle of the applied potential of 6 kV peak-to-peak (black dashed lines) at a frequency of 20 kHz.

As can be seen from figure 10A, for helium DBD with no packing, the current profile exhibits a single distinct pulse in the positive half cycle of the applied voltage. In the negative half cycle, discharge current shows multiple peaks, with the first peak being of higher amplitude followed by six peaks of much smaller amplitudes. As opposed to DBD with no packing, the discharge current profile for DBD with partial packing (figure 10B) shows multiple peaks in both the positive and negative half cycles of applied voltage, showing characteristics of a pseudoglow discharge. In addition, the amplitude of the peaks are also higher in both positive and negative voltage cycle, signifying a stronger discharge. The discharge current profile shows five peaks of varying amplitude, marked 1-5 in the figure 10B, with peaks 1,2 and 4 of much higher amplitude than peaks 3 and 5. Similar increase in number of peaks on inclusion of packing materials has been observed before in various experimental studies[16,41]. Higher applied potential induces higher electric field strength in the discharge gap, increasing the chances of multiple gas breakdown. Such an irregular multipeak behaviour occurs due to independent discharges occurring in different parts of the reactor progressively depending on the electric field strength in a given region at given time. Similar behaviour was also observed in the numerical study of fully packed DBDs by

Van Laer and Bogaerts[21] at applied potential of 7.5 kV peak-to-peak. The current profile in the negative half cycle of the applied voltage is similar for both DBD configurations, except for the fact that the amplitude of the first major peak for DBD with partial packing is almost double of that obtained for DBD with no packing.

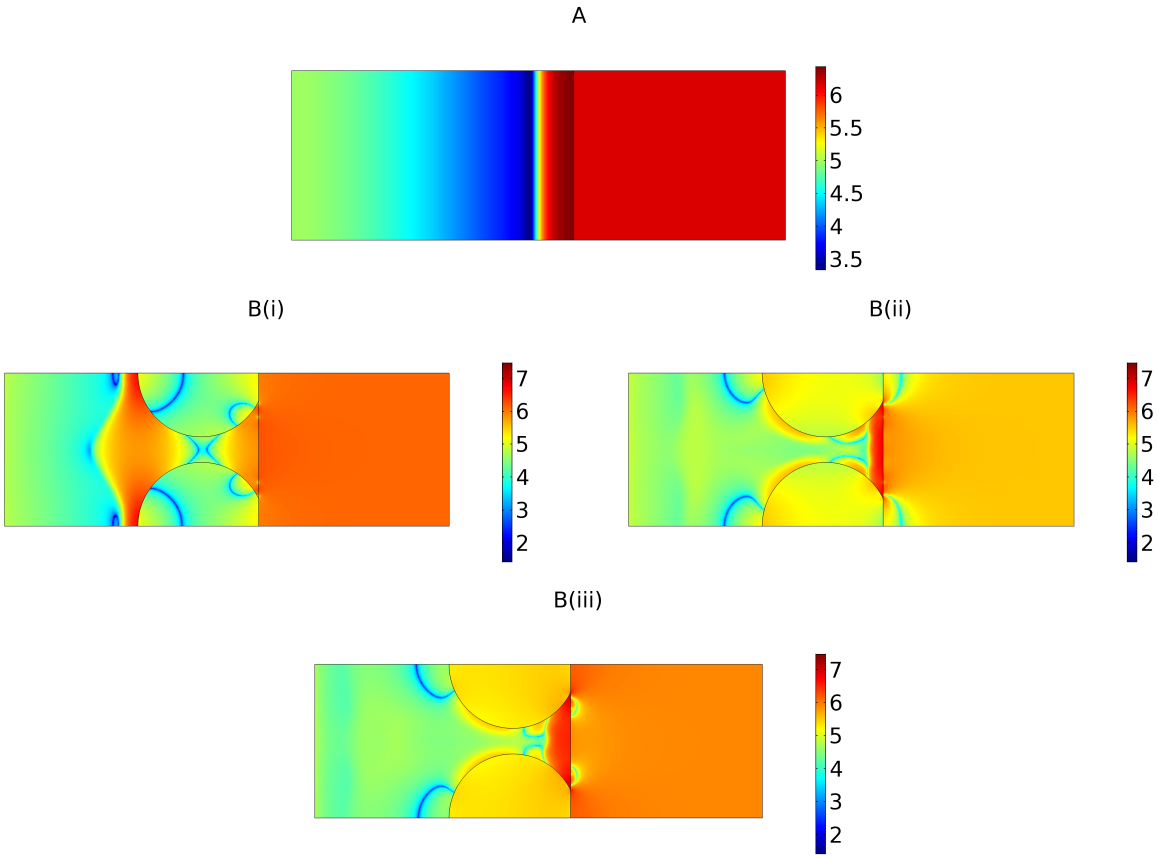

FIG. 11. Logarithm to the base 10 of electric field strength (V/m) at the moment of gas breakdown in (A) DBD with no packing, corresponding to time at major current peak from figure 10A and (B) DBD with partial packing corresponding to times at the three current peaks at (Bi) peak 1, (Bii) peak 2 and (Biii) peak 4 from figure 10B.

Figures 11, 12 and 13 show the electric field, electron number density, and ion number density distributions at the particular moments of breakdown during the positive half cycle of the voltage period, corresponding to times shown in figure 10 for both DBD configurations. In all the three figures, for DBD with no packing, we have plotted the distribution profiles for the first major peak corresponding to the breakdown moment observed in discharge current

profile in figure 10A, which are represented as plot A in figures 11, 12 and 13. For DBD with partial packing however, we have plotted the distribution profiles for the three major peaks (1,2 and 4) corresponding to breakdown moments observed in discharge current profile in figure 10B, which are represented as plots B (i, ii, & iii) in figures 11, 12 and 13.

As can be seen in figures 11A, 12A and 13A, for DBD without any packing, electron density, electron number density, and ion number density distributions at the moment of breakdown during the positive half cycle of the voltage period for higher applied potential of 6 kV are similar to that observed for lower applied potential of 3 kV, with an expected increase in magnitude due to higher input power. These profiles also show characteristics of APGD with three distinct regions, cathode fall, negative glow space, and positive column region.

For DBD with partial packing, electric field distribution at first major peak (figure 11 B(i)), shows a higher electric field strength at the top surface of the packing particles and for peaks 2 (figure 11 B(ii)) and 4 (figure 11 B(iii)) the maximum electric field strength is observed at the two contact points between packing and dielectric layer, and in the region of discharge between the contact points touching the dielectric layer. Also, for DBD with partial packing, the electric field strength at the three major peaks is slightly higher than that observed at the major peak for DBD with no packing. As can be seen in figure 10, the current pulses spread over more than half of the discharge current profile, providing regions of high electric field strength (as seen in figure 11) for a larger section and longer time of discharge in the positive half cycle of the applied voltage.

Figures 12 B(i), B(ii), and B(iii) show the electron density distributions at the three breakdown moments (peak 1, 2 and 4) during the positive half cycle of the applied voltage as seen in figure 10B for DBD with partial packing. For higher applied potential 6 kV peak-to-peak, the maximum electron density distributions corresponding to the three peaks of discharge current profile for DBD with partial packing (figures 12 B(i), B(ii) and B(iii)), are roughly about one magnitude higher than that obtained for DBD with no packing (figure 12 A). The maximum electron density for the peak 2 (figure 12 B(ii))) is slightly higher ($\sim$ 6.5x10^{12} cm^{-3}) compared to that obtained for peak 1 ($\sim$ 1.7x10^{12} cm^{-3}) and peak 4 ($\sim$ 2.5x10^{12} cm^{-3}), for DBD with partial packing. Comparatively, the maximum electron density for DBD with no packing ($\sim$ 5x10^{11} cm^{-3}) obtained at the moment of breakdown is lower than the maximum electron density observed for peaks 1, 2 and 4 for DBD with

partial packing. For peak 1 ((figure 12 B(i)), the maximum electron density is observed near the top surface of two particles, just after a low electron density region in the shape of a pointy knob upwards from the dielectric barrier layer, signifying a cathode fall region at the moment of breakdown. The electron density distributions corresponding to the peaks 2 and 4 ((figures 12 B(ii) and B(iii)), exhibit cylindrical regions of high electron electron density in the regions between the two particles. It should be pointed out that the higher applied potential of 6 kV peak-to-peak indeed extends the region of high intensity electron density distributions compared to that observed with applied potential of 3 kV. This is a result of the higher number of breakdowns in the current profile obtained at the applied voltage of 6 kV peak-to-peak.

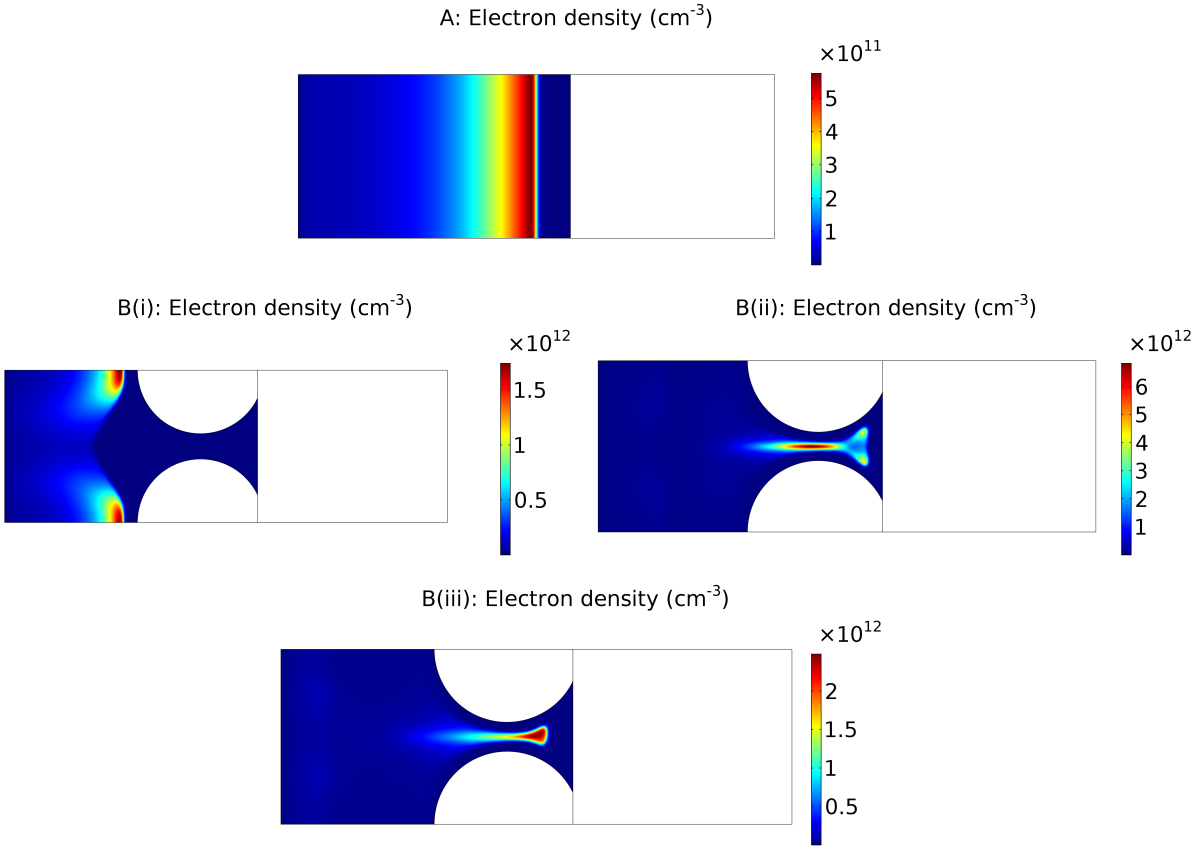

FIG. 12. Electron Density (cm^{-3}) at the moment of gas breakdown in (A) DBD with no packing, corresponding to time at major current peak from figure 10A and (B) DBD with partial packing corresponding to times at the three current peaks at (Bi) peak 1, (Bii) peak 2 and (Biii) peak 4 from figure 10B.

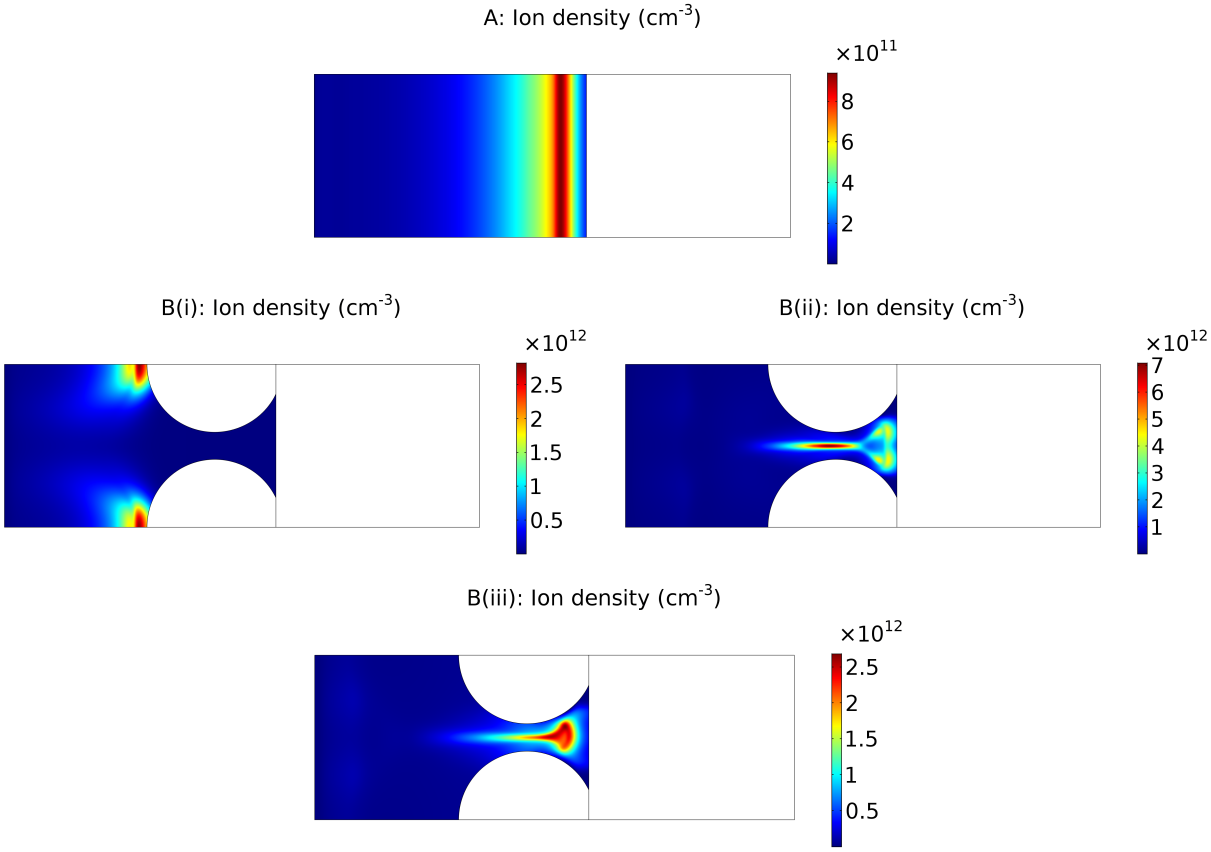

FIG. 13. Ion Density (cm^{-3}) at the moment of gas breakdown in (A) DBD with no packing, corresponding to time at major current peak from figure 10A and (B) DBD with partial packing corresponding to times at the three current peaks at (Bi) peak 1, (Bii) peak 2 and (Biii) peak 4 from figure 10B.

Figures 13 B(i), B(ii), and B(iii) show the ion density distributions at the three breakdown moments (peak 1, 2 and 4) during the positive half cycle of the applied voltage as seen in figure 10B for DBD with partial packing. The ion density distributions reproduce similar profiles as obtained for electron density distribution (figure 12) at the three peaks, except for the low intensity region of cathode fall. The maximum ion density at the three peaks for DBD with partial packing is about one magnitude higher than that obtained for DBD with no packing, suggesting a much stronger ionization on inclusion of packing. Also, similar to what was observed for applied potential of 3 kV, even at the higher applied potential of 6 kV, the ion densities (figure 13) at the breakdown moments are always higher compared to the electron densities (figure 12) for both DBD configurations with and without packing.

As mentioned before, this is an important feature of APGD. Also, the electron and ion densities though higher at applied potential of 6 kV, are still within the range of typical values observed for APGD.

The space charge density profiles for applied potential of 6 kV peak-to-peak (not shown here) follow the same pattern as the ion density distributions (figure 13), suggesting the movement of charges from the top surface of packing beads to the region between the beads close to the dielectric layer, leading to the multiple breakdowns in discharge current, manifested as various peaks in figure 10B.

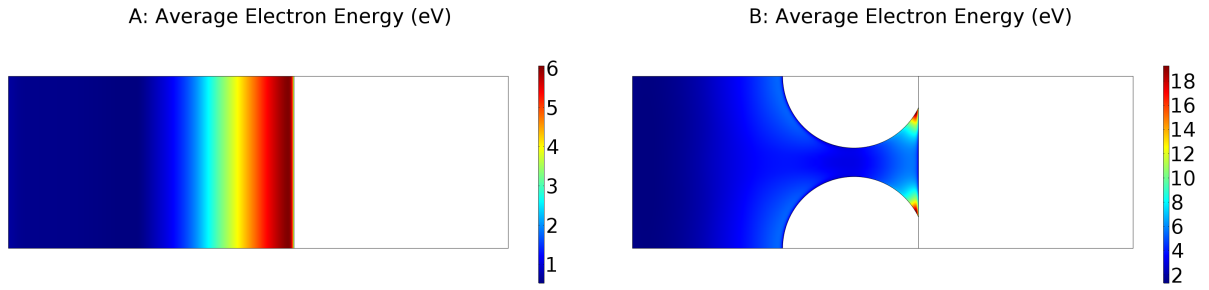

FIG. 14. Time averaged electron energy (eV) distribution during the positive half cycle for applied potential of 6.0 kV peak-to-peak as shown in figure 10 for (A) DBD with no packing and (B) DBD with partial packing.

Figure 14 shows the time averaged electron energy distribution during the positive half cycle of applied potential 6.0 kV peak-to-peak for both DBD configurations. Comparing with figure 9, the average electron energy at applied potential of 6 kV is higher than that obtained for applied potential of 3 kV, for both the DBD configurations with and without packing. For DBD with no packing (figure 14A), the maximum electron energy during the half voltage cycle is about 6eV and is observed near the instantaneous cathode close to the dielectric surface. On the other hand, for DBD with partial packing (figure 14B), the maximum electron energy during the half voltage cycle is close to 18 eV, which is three times of that obtained for DBD with no packing. In the average plot (figure 14B), the highest intensity of electron energy is observed at the contact points between the packing material and the dielectric barrier. The average electron energy in the vicinity of the packing surface is about 5-10 eV. This local enhancement in electron energy at the contact points and near the surface of the packing is obtained due to the augmentation of the electric

field strength in these regions. It should be noted that compared to the applied potential of 3 kV peak-to-peak, where the maximum of the average electron energy for DBD with partial packing increased twice that of DBD with no packing, at higher electron potential of 6 kV, the increase in the average electron energy is much more pronounced for DBD with partial packing. The multiple breakdowns in the discharge at higher applied potential (6 kV), lead to a much longer and wider distribution of the high intensity discharge compared to that obtained at lower applied potential (3 kV), which can lead to the substantially higher electron energy distribution at applied potential of 6 kV.

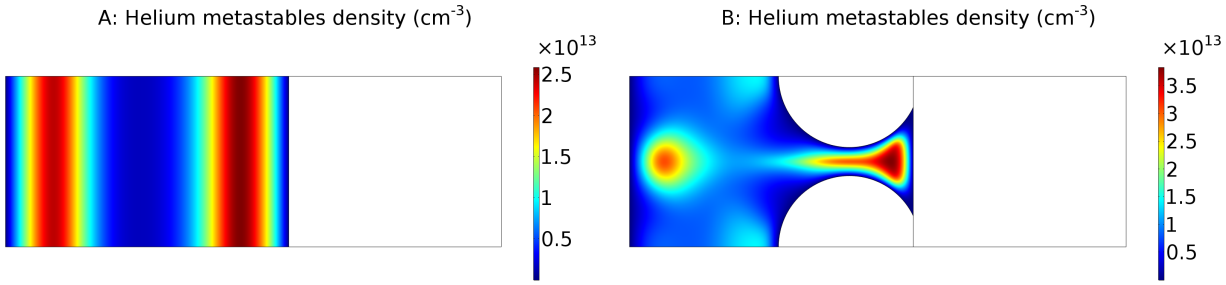

FIG. 15. Time averaged helium metastable atoms (He^* and He_2^*) density distribution during the positive half cycle for applied potential of 6.0 kV peak-to-peak as shown in figure 10 for (A) DBD with no packing and (B) DBD with partial packing.

Energetic and excited metastable helium atoms (He^* and He_2^*) produced in the plasma discharge can interact with impurities in the helium gas (nitrogen or oxygen). Since most impurities have an ionization potential lower than the threshold of metastable states, they can be easily ionized via the so-called penning effect[44,45]. Even though this study considers a pure helium gas, it is interesting to see if the addition of partial packing leads to any change in the density of metastable helium atoms or its distribution. This information will provide a rough estimate of the potential penning ionization contribution towards increasing the ionization coefficient of the reactor given the percentage of impurities is equal in the two DBD configurations.

Figure 15 shows the time averaged helium metastable atoms density distribution during the positive half cycle of applied potential 6.0 kV peak-to-peak for both DBD configurations. As can be seen from the figure, the time averaged distribution of helium metastable atoms density is quite different in the two configurations. For DBD with no packing, high density

of metastable helium atoms is observed near the two boundaries of the discharge space. On the other hand, for DBD with partial packing, the metastable helium atoms are seen to be concentrated in the gap between the two packing beads and at the center point directly opposite this gap, close to the boundary of the inner cylinder. Region close to the top surface of the packing beads also have a relative high density of metastable atoms compared to the remaining of the discharge space. It should however be noted that though the distribution of metastable atoms density changes considerably on addition of partial packing, the magnitude of the time averaged density is roughly same in both DBD configurations. Time averaged metastable atoms density for lower applied potential of 3 kV peak-to-peak (not shown here) has a similar distribution for both DBD with no packing and DBD with partial packing.

In addition to electron density and electron energy, power consumption of the discharge is also an important indicator of the performance and energy efficiency of the DBD reactor. The average power density over a period T is obtained by integrating the instantaneous power dissipated in the system, as follows

$$\bar{P} = \frac{1}{T}\int_0^T V_{gap}(t) I_{cond}(t) dt \tag{12}$$

where, V_{gap} and I_{cond} represent the gap voltage and conduction current respectively.

Table I shows the spatially and time averaged dissipated power density, electron density and electron energy for one voltage cycle, at different applied voltage amplitudes for both the DBD configurations (without packing and with partial packing).

TABLE I. Spatially and time averaged dissipated power density (W m^{-3}) and electron density (cm^{-3}) and electron energy (eV) for one voltage cycle at different applied voltage amplitudes and DBD configurations for applied frequency 20 kHz

Applied potential/DBD configuration	Power density W m^{-3}	Electron density cm^{-3}	Electron energy eV
3 kV / No Packing	2.75x10^5	2.39x10^{10}	2.11
3 kV / Partial Packing	4.17x10^5	2.17x10^{10}	3.20
6 kV / No Packing	6.80x10^5	2.39x10^{10}	2.24
6 kV / Partial Packing	1.02x10^6	2.23x10^{10}	3.24

As can be seen from table I, when the applied voltage potential is increased from 3 kV to 6 kV, the spatially and time averaged power density over one voltage cycle also increases ($\sim$ 150 %) for both DBD configurations. The power density is also found to be increasing when

a partial packing is added to the DBD, for applied potential of both 3 kV and 6 kV. The percentage increase in power density on addition of packing is approximately same ($\sim$ 50 %) at both values of applied potential. The spatially and time averaged electron density over one voltage cycle is seen to be of roughly similar magnitude (of the order $1x10^{10}$) at different applied potential (3 kV or 6 kV) and DBD configurations (no packing/ partial packing). This is in accordance with previously reported work by Tu et. al.[41], who calculated the average electron density from electrical parameters for helium DBD and found that partial radial packing of Al_2O_3 had little effect on the average electron density. However it should be noted that in this work, we have used the axial partial packing and addition of partial packing is seen to slightly reduce (although no change in order of magnitude) the average electron density values for applied voltage of both 3 kV and 6 kV.

In addition to the electron density, the DBD reactor performance is also influenced by the total number of electrons present in the reactor. This factor may become more significant in the current study, as the volume of the reactor is reduced due to the addition of partial packing. To obtain the total electron count, the volume of DBD reactor with no packing and for DBD with partial packing is calculated based on the dimensions of the DBD reactor and packing beads, and multiplied to the spatially and time averaged electron density over one voltage cycle as described in table I. Please note that the volume of DBD with partial packing is calculated by subtracting the total volume occupied by the beads from the volume of the discharge space of DBD with no packing. Based on the calculations, the total electron number count for DBD with no packing and DBD with partial packing is $2.70x10^{11}$ and $2.44x10^{11}$ respectively for applied potential of 3 kV peak-to-peak. The same at higher potential of 6 kV is $2.70x10^{11}$ and $2.51x10^{11}$ respectively. As can be seen, similar to electron density even the total electron count for the two DBD configurations are of similar magnitude for both values of applied potential. This is mainly because the volume displaced by the addition of partial packing is a very small fraction compared of the total volume of the DBD reactor. In the case of a fully packed DBD reactor however, the volume displaced by the packing is significantly higher and this is known to change the discharge characteristics[16].

It can also be seen from table I that spatially and time averaged electron energy over one voltage cycle increases on inclusion of partial packing ($\sim$ 45-50 %) at both applied potential values. The spatially and time averaged electron energy also shows a small increase as the applied potential is raised from 3 kV to 6 kV (peak-to-peak) for both DBD configurations.

All the above results suggest that addition of partial packing enhances the electric field strength and creates a stronger discharge without making any significant change to the discharge mode of the DBD. Together the cumulative effect of higher surface area, enhanced electric field strength, higher electron and ion densities and a broader range of electron energy will result in an increased production of excited species for the partially packed DBD as compared to DBD without any packing, for the same input power. This is in accordance with the experimental results observed by Tu and Whitehead[16]. When implemented in applications for gas cleaning or chemical synthesis, production of higher density of excited species and free radicals in a partially packed DBD, can result in better performance as compared to a DBD with no packing. For the helium DBD studied in this work, the discharge at lower applied potential of 3 kV peak-to-peak is found to be localized. However increasing the applied potential to 6 kV peak-to-peak, resulted in higher charge deposition and multiple breakdowns, particularly in partially packed DBD, which thereby lead to a more spread-out distribution of the high intensity discharge.

It should be noted that in the given configuration of the partially packed DBD, the packing particles are placed only on one side of the co-axial discharge gap. This creates asymmetry in the geometry and prevents one from using a 2D-axi-symmetrical model, that can give a more accurate representation of the 3D co-axial discharge gap. The 2D geometry used in the model is only an approximation of the co-axial discharge space and neglects a substantial section of the co-axial gap which does not interact with any packing. This is a limitation of the 2D model used in this work. Thus the results obtained in this study have to be viewed with caution and it should be presumed that the actual change in overall discharge characteristics of the DBD may be less dramatic than what is observed here. It should also be noted that there can be many different configurations in which partial packing can be introduced in a DBD, such as radial partial packing, axial partial packing, more than one column (line) of packing at the bottom of the dielectric tube, etc. The results of this study are limited to the axial packing method as described in figure 1. However the understanding developed through this study will certainly be helpful in improving our insight of the ways in which packing materials interact and influence the plasma discharge in DBDs. More extensive investigations, comparing different packing configurations in a DBD (including fully packed DBD) and specific experimental studies for more quantitative comparison of discharge parameters, needs to be carried to explore the full capabilities of DBD reactors.

A comprehensive study comparing the discharge characteristics of a fully packed DBD with a partially packed DBD, along with focused experimental studies are planned for the near future.

IV. CONCLUSION

In this work, a numerical analysis of co-axial DBD in pure helium has been carried out using 2-D fluid model. This model has been used to understand the influence of partial packing on the discharge characteristics of the DBD and the changes are assessed by comparing the results with those obtained using a plasma-alone DBD reactor with no packing. The model is first validated by comparing the predicted discharge current profile with that reported in an experimental study from literature for a helium DBD with no packing.

The discharge performance is then studied at two values of applied potential (3 kV and 6 kV peak-to-peak) at a fixed frequency of 20 kHz for both the DBD configurations. At the lower potential (3 kV peak-to-peak), the discharge current profile for DBD with no packing shows single distinct peaks in the positive and negative half cycles of voltage. Inclusion of partial packing, leads to an increase in the number of peaks in the discharge current profile in the positive half cycle. At higher potential (6 kV peak-to-peak) the number of peaks increases further due to more effective polarization at the contact points leading to multiple breakdowns in a single voltage cycle. In addition to increase in the number of peaks, the amplitude of the major peak also increases in the discharge current profiles, suggesting a stronger discharge with partial packing as opposed to no packing.

Electric field distribution profiles at the moments of breakdown, show an enhancement at the top surface of the spherical packing material and at the contact points between packing and dielectric layer. The multiple breakdowns in the discharge at higher applied potential (6 kV), lead to a much longer and wider distribution of the high intensity discharge compared to that obtained at lower applied potential (3 kV). This enhancement is also reflected in the values of electron and ion number densities at the moments of breakdown, which consistently show higher values for DBD with partial packing as compared to DBD with no packing at the breakdown moments for both applied potentials.

The time averaged electron energy distribution during the positive half cycle of applied voltage for DBD with partial packing shows region of high intensity in the vicinity of the

packing materials and at the contact points. At both applied potential values, the time averaged electron energy distribution shows that much higher electron energy could be achieved with partial packing, as compared to DBD with no packing, using the same applier power. Spatially and time averaged discharge parameters show an increase in power density and electron energy with increase in potential as well as on inclusion of partial packing. The results presented in this study offer new insights in understanding the influence of partial packing in a DBD reactor and suggest the possible factors that may cause the relatively better performance observed in experiments when compared to a DBD with no packing.

ACKNOWLEDGMENTS

The authors would like to gratefully acknowledge the Engineering and Physical Sciences Research Council (EPSRC) UK for the financial support of this work through EPSRC grants EP/M013162/1 and EP/K036548/2.

REFERENCES

[1]M.B. Chang and H.M. Lee. Abatement of perfluorocarbons with combined plasma catalysis in atmospheric-pressure environment. *Catal. Today*, 89(1-2):109–115, 2004.

[2]J. Van Durme, J. Dewulf, C. Leys, and H. Van Langenhove. Combining non-thermal plasma with heterogeneous catalysis in waste gas treatment: A review. *Appl. Catal., B*, 78(3-4):324–333, 2008.

[3]J.C. Whitehead. Plasma catalysis: A solution for environmental problems. *Pure Appl. Chem.*, 82(6):1329–1336, 2010.

[4]Paul K Chu and XinPei Lu. *Low temperature plasma technology: methods and applications*. CRC Press, 2013.

[5]K. Urashima and J.-S. Chang. Removal of volatile organic compounds from air streams and industrial flue gases by non-thermal plasma technology. *IEEE Trans. Dielectr. Electr. Insul.*, 7(5):602–614, 2000.

[6]H.L. Chen, H.M. Lee, S.H. Chen, Y. Chao, and M.B. Chang. Review of plasma catalysis on hydrocarbon reforming for hydrogen production-interaction, integration, and prospects. *Appl. Catal., B*, 85(1-2):1–9, 2008.

[7]H.-H. Kim. Nonthermal plasma processing for air-pollution control: A historical review, current issues, and future prospects. *Plasma Processes Polym.*, 1(2):91–110, 2004.

[8]C.-L. Chang and T.-S. Lin. Decomposition of toluene and acetone in packed dielectric barrier discharge reactors. *Plasma Chem. Plasma Process.*, 25(3):227–243, 2005.

[9]B. Eliasson, C.-J. Liu, and U. Kogelschatz. Direct conversion of methane and carbon dioxide to higher hydrocarbons using catalytic dielectric-barrier discharges with zeolites. *Ind. Eng. Chem. Res.*, 39(5):1221–1227, 2000.

[10]Martin Kraus, Baldur Eliasson, Ulrich Kogelschatz, and Alexander Wokaun. Co2 reforming of methane by the combination of dielectric-barrier discharges and catalysis. *Phys. Chem. Chem. Phys.*, 3:294–300, 2001.

[11]Debjyoti Ray and Ch. Subrahmanyam. Co2 decomposition in a packed dbd plasma reactor: influence of packing materials. *RSC Adv.*, 6:39492–39499, 2016.

[12]A.-J. Zhang, A.-M. Zhu, J. Guo, Y. Xu, and C. Shi. Conversion of greenhouse gases into syngas via combined effects of discharge activation and catalysis. *Chem. Eng. J.*, 156(3): 601–606, 2010.

[13]H.K. Song, J.-W. Choi, S.H. Yue, H. Lee, and B.-K. Na. Synthesis gas production via dielectric barrier discharge over ni/-al2o3 catalyst. *Catal. Today*, 89(1-2):27–33, 2004.

[14]X. Tu, H.J. Gallon, M.V. Twigg, P.A. Gorry, and J.C. Whitehead. Dry reforming of methane over a ni/al2o3 catalyst in a coaxial dielectric barrier discharge reactor. *J. Phys. D: Appl. Phys.*, 44(27):274007, 2011.

[15]K. Zhang, B. Eliasson, and U. Kogelschatz. Direct conversion of greenhouse gases to synthesis gas and c4 hydrocarbons over zeolite hy promoted by a dielectric-barrier discharge. *Ind. Eng. Chem. Res.*, 41(6):1462–1468, 2002.

[16]X. Tu and J.C. Whitehead. Plasma-catalytic dry reforming of methane in an atmospheric dielectric barrier discharge: Understanding the synergistic effect at low temperature. *Appl. Catal., B*, 125:439–448, 2012.

[17]H.J. Gallon, X. Tu, and J.C. Whitehead. Effects of reactor packing materials on h 2 production by co 2 reforming of ch 4 in a dielectric barrier discharge. *Plasma Processes Polym.*, 9(1):90–97, 2012.

[18]X. Tu, H.J. Gallon, and J.C. Whitehead. Electrical and spectroscopic diagnostics of a single-stage plasma-catalysis system: Effect of packing with tio2. *J. Phys. D: Appl. Phys.*, 44(48):482003, 2011.

[19]D. Mei, B. Ashford, Y.-L. He, and X. Tu. Plasma-catalytic reforming of biogas over supported ni catalysts in a dielectric barrier discharge reactor: Effect of catalyst supports. *Plasma Processes Polym.*, 14(6):e201600076, 2017.

[20]D. Mei, X. Zhu, C. Wu, B. Ashford, P.T. Williams, and X. Tu. Plasma-photocatalytic conversion of co2 at low temperatures: Understanding the synergistic effect of plasma-catalysis. *Appl. Catal., B*, 182:525–532, 2016.

[21]K. Van Laer and A. Bogaerts. Fluid modelling of a packed bed dielectric barrier discharge plasma reactor. *Plasma Sources Sci. Technol.*, 25(1):015002, 2015.

[22]J.C. Whitehead. Plasma-catalysis: The known knowns, the known unknowns and the unknown unknowns. *J. Phys. D: Appl. Phys.*, 49(24):243001, 2016.

[23]E.C. Neyts, K. Ostrikov, M.K. Sunkara, and A. Bogaerts. Plasma catalysis: Synergistic effects at the nanoscale. *Chem. Rev.*, 115(24):13408–13446, 2015.

[24]A.M. Vandenbroucke, R. Morent, N. De Geyter, and C. Leys. Non-thermal plasmas for non-catalytic and catalytic voc abatement. *J. Hazard. Mater.*, 195:30–54, 2011.

[25]E.C. Neyts and A. Bogaerts. Understanding plasma catalysis through modelling and simulation - a review. *J. Phys. D: Appl. Phys.*, 47(22):224010, 2014.

[26]W.S. Kang, J.M. Park, Y. Kim, and S.H. Hong. Numerical study on influences of barrier arrangements on dielectric barrier discharge characteristics. *IEEE Trans. Plasma Sci.*, 31 (4 II):504–510, 2003.

[27]J. Kruszelnicki, K.W. Engeling, J.E. Foster, Z. Xiong, and M.J. Kushner. Propagation of negative electrical discharges through 2-dimensional packed bed reactors. *J. Phys. D: Appl. Phys.*, 50(2):025203, 2017.

[28]D. Marinov, C. Teixeira, and V. Guerra. Deterministic and monte carlo methods for simulation of plasma-surface interactions. *Plasma Processes Polym.*, 14(1-2):1600175, 2017.

[29]www.comsol.com.

[30]H. Russ, M. Neiger, and J.E. Lang. Simulation of micro discharges for the optimization of energy requirements for removal of no x from exhaust gases. *IEEE Trans. Plasma Sci.*, 27(1):38–39, 1999.

[31]K. Takaki, J.S. Chang, and K.G. Kostov. Atmospheric pressure of nitrogen plasmas in a ferroelectric packed bed barrier discharge reactor. part i. modeling. *IEEE Trans. Dielectr. Electr. Insul.*, 11(3):481–490, 2004.

[32]K. Van Laer and A. Bogaerts. Influence of gap size and dielectric constant of the packing material on the plasma behaviour in a packed bed dbd reactor: A fluid modelling study. *Plasma Processes Polym.*, 2016. doi:10.1002/ppap.201600129.

[33]Y. Zhang, H.-Y. Wang, W. Jiang, and A. Bogaerts. Two-dimensional particle-in cell/monte carlo simulations of a packed-bed dielectric barrier discharge in air at atmospheric pressure. *New J. Phys.*, 17(8):083056, 2015.

[34]R. Snoeckx, Y. X. Zeng, X. Tu, and A. Bogaerts. Plasma-based dry reforming: improving the conversion and energy efficiency in a dielectric barrier discharge. *RSC Adv.*, 5:29799–29808, 2015.

[35]P. Talebizadeh, H. Rahimzadeh, M. Babaie, S.J. Anaghizi, H. Ghomi, G. Ahmadi, and R. Brown. Evaluation of residence time on nitrogen oxides removal in non-thermal plasma reactor. *PLoS ONE*, 10(10):0140897, 2015.

[36]M.M. Gomaa and H.M. Gobara. Electrical properties of ni/silica gel and pt/-alumina catalysts in relation to metal content in the frequency domain. *Mater. Chem. Phys.*, 113 (2-3):790–796, 2009.

[37]G.G. Raju. *Gaseous Electronics: Tables, Atoms, and Molecules*. CRC Press, 2011.

[38]Yu.B. Golubovskii, V.A. Maiorov, J. Behnke, and J.F. Behnke. Modelling of the homogeneous barrier discharge in helium at atmospheric pressure. *J. Phys. D: Appl. Phys.*, 36 (1):39–49, 2003.

[39]S. K Jhala, P. B.; Nema. *Plasma Technologies for Textile and Apparel*. Woodhead Publishing India in textiles. WPI India, 2014. ISBN 978-93-80308-95-1,9380308957.

[40]F. Iza, S. H. Lee, and J. K. Lee. Computer modeling of low-temperature plasmas. In J. A. Filho, editor, *Gas discharges : fundamentals & applications*, Thin Films and Nanostructures, pages 1 – 31. Transworld Research Work, 2007.

[41]X. Tu, B. Verheyde, S. Corthals, S. Paulussen, and B.F. Sels. Effect of packing solid material on characteristics of helium dielectric barrier discharge at atmospheric pressure. *Phys. Plasmas*, 18(8):080702, 2011.

[42]S. Kanazawa, M. Kogoma, T. Moriwaki, and S. Okazaki. Stable glow plasma at atmospheric pressure. *J. Phys. D: Appl. Phys.*, 21(5):838–840, 1988.

[43]S. Gadkari and S. Gu. Numerical investigation of co-axial dbd: Influence of relative permittivity of the dielectric barrier, applied voltage amplitude, and frequency. *Phys. Plasmas*, 24(5):053517, 2017.

[44]D. Petrović, T. Martens, J. Van Dijk, W.J.M. Brok, and A. Bogaerts. Fluid modelling of an atmospheric pressure dielectric barrier discharge in cylindrical geometry. *J. Phys. D: Appl. Phys.*, 42(20):205206, 2009.

[45]I. Radu, R. Bartnikas, and M.R. Wertheimer. Frequency and voltage dependence of glow and pseudoglow discharges in helium under atmospheric pressure. *IEEE Trans. Plasma Sci.*, 31(6 II):1363–1378, 2003.

[46]D. Wang, Y. Wang, and C. Liu. Multipeak behavior and mode transition of a homogeneous barrier discharge in atmospheric pressure helium. *Thin Solid Films*, 506-507:384–388, 2006.

[47]F. Massines, N. Gherardi, N. Naudé, and P. Ségur. Recent advances in the understanding of homogeneous dielectric barrier discharges. *EPJ Appl. Phys.*, 47(2), 2009.

[48]H.-Y. Zhang, D.-Z. Wang, and X.-G. Wang. Numerical studies of atmospheric pressure glow discharge controlled by a dielectric barrier between two coaxial electrodes. *Chinese Phys.*, 16(4):1089–1096, 2007.

[49]Y.T. Zhang, D.Z. Wang, and M.G. Kong. Two-dimensional simulation of a low-current dielectric barrier discharge in atmospheric helium. *J. Appl. Phys.*, 98(11), 2005.

[50]N.Yu. Babaeva, D.V. Tereshonok, G.V. Naidis, and B.M. Smirnov. Streamer branching on clusters of solid particles in air and air bubbles in liquids. *J. Phys.: Conf. Ser.*, 774(1): 012151, 2016.

[51]D.K. Cheng. *Field and Wave Electromagnetics*. The Addison-Wesley series in electrical engineering. Addison-Wesley Publishing Company, 1989. ISBN 9780201528206.

[52]A. Gmez-Ramrez, A. Montoro-Damas, M.A. Rodrguez, A. Gonzlez-Elipe, and J. Cotrino. Improving the pollutant removal efficiency of packed-bed plasma reactors incorporating ferroelectric components. *Chem. Eng. J.*, 314:311–319, 2017.

[53]Alexander Fridman. Electric discharges in plasma chemistry. In *Plasma Chemistry:*, pages 157–258. Cambridge University Press, Cambridge, 005 2008.

[54]D. Lee, J.M. Park, S.H. Hong, and Y. Kim. Numerical simulation on mode transition of atmospheric dielectric barrier discharge in helium-oxygen mixture. *IEEE Trans. Plasma Sci.*, 33(2 III):949–957, 2005.